# Efficient Approximation of Potential Energy Surfaces with Mixed-Basis Interpolation

Zachary Morrow,† Hyuk-Yong Kwon,‡ C. T. Kelley,\*,† and Elena Jakubikova\*,‡

†Department of Mathematics, North Carolina State University, Raleigh, NC 27695 ‡Department of Chemistry, North Carolina State University, Raleigh, NC 27695

E-mail: tim\_kelley@ncsu.edu; ejakubi@ncsu.edu

#### Abstract

The potential energy surface (PES) describes the energy of a chemical system as a function of its geometry and is a fundamental concept in modern chemistry. A PES provides much useful information about the system, including the structures and energies of various stationary points, such as stable conformers (local minima) and transition states (first-order saddle points) connected by a minimum-energy path. Our group has previously produced surrogate reduced-dimensional PESs using sparse interpolation along chemically significant reaction coordinates, such as bond lengths, bond angles, and torsion angles. These surrogates used a single interpolation basis, either polynomials or trigonometric functions, in every dimension. However, relevant molecular dynamics (MD) simulations often involve some combination of both periodic and nonperiodic coordinates. Using a trigonometric basis on nonperiodic coordinates, such as bond lengths, leads to inaccuracies near the domain boundary. Conversely, polynomial interpolation on the periodic coordinates does not enforce the periodicity of the surrogate PES gradient, leading to nonconservation of total energy even in a microcanonical ensemble. In this work, we present an interpolation method that uses trigonometric interpolation on the periodic reaction coordinates and polynomial interpolation on the

nonperiodic coordinates. We apply this method to MD simulations of possible isomerization pathways of azomethane between *cis-* and *trans-* conformers. This method is the only known interpolative method that appropriately conserves total energy in systems with both periodic and nonperiodic reaction coordinates. In addition, compared to all-polynomial interpolation, the mixed basis requires fewer electronic structure calculations to obtain a given level of accuracy, is an order of magnitude faster, and is freely available on GitHub.

## 1 Introduction

The potential energy surface (PES) of a molecule maps its geometry to a corresponding electronic energy within the Born–Oppenheimer approximation. Born and Oppenheimer [1927], Born and Fock [1928], Born and Huang [1954] One can glean much chemically useful information from a PES: local minima and first-order saddle points correspond to stable and transition-state structures respectively, from which one may calculate energy barriers and minimum-energy paths that describe chemical reactivity. Such knowledge is useful for both theoretical investigations Glasstone et al. [1941] as well as molecular dynamics (MD) simulations. Albaugh et al. [2016], Brown et al. [2003], Bowman et al. [2011], Liu et al. [2019], Nance et al. [2014] Highly accurate evaluations of a PES can be done with an ab initio and density functional theory (DFT) methods, but the computational cost of these methods rises rapidly with the number of atoms N. For instance, the computational cost of DFT scales as  $\mathcal{O}(N^3)$ , while second-order Møller–Plesset perturbation theory (MP2) is  $\mathcal{O}(N^5)$  and coupled cluster with single and double excitations (CCSD) is  $\mathcal{O}(N^6)$ . Koch and Holthausen [2001] Thus, if a large number of PES evaluations is required, a surrogate PES becomes necessary.

Various techniques exist to construct surrogate PESs, such as modified Shepard interpolation, Collins and Parsons [1993], Collins [2002, 2003], Thompson et al. [1998], Espinosa-Garcia et al. [2012], Wu and Manthe [2003], Zhou et al. [2011] permutationally invariant polynomials (PIP), Albaugh et al. [2016], Brown et al. [2003], Bowman et al. [2011], Braams and Bow-

man [2009], Chen and Bowman [2018], Qu et al. [2018] interpolative moving least-squares (IMLS),Dawes and Quintas-Sánchez [2018], Guo et al. [2007], McLain [1974], Farwig [1986], Maisuradze et al. [2003] Gaussian processes,Cui and Krems [2015], Uteva et al. [2017] neural networks (nn-PES),Jiang et al. [2016], Lorenz et al. [2004], Manzhos et al. [2014], Lin et al. [2021], Schran et al. [2020] and the finite-element method.Berweger et al. [1998] Most of these methods are primarily concerned with constructing a full PES as a function of 3N-6 internal coordinates representing bond lengths, bond angles, and torsion angles. Even with an *ab initio* method that has relatively low cost scaling, these full-dimensional surrogates are feasible only for small atoms (i.e.,  $N \leq 10$ ).

Fortunately, often only a subset of the 3N-6 internal coordinates (called design variables) are chemically relevant for a particular system. The rest of the internal coordinates (the remainder variables) are optimized to yield the minimum electronic energy for a fixed value of the design variables. The resulting PES is called a relaxed PES. Even with relaxation, however, optimizing the remainder variables is often computationally costly.

Our group has previously approximated relaxed PESs with sparse polynomial interpolation, a method chosen for advantageous scaling in the dimensionality of the PES compared to other methods discussed above. Nance and Kelley [2015], Judd et al. [2014] Here, the interpolation basis functions are globally defined Lagrange polynomials with the Clenshaw—Curtis points. Clenshaw and Curtis [1960] The global nature of the basis functions is also a distinction between this method and modified Shepard interpolation or interpolative moving least squares, which use a spatially weighted combination of locally valid basis functions. Thompson et al. [1998], Maisuradze et al. [2003] Furthermore, the Smolyak sparse-grid frameworkSmolyak [1963] ensures that the total number of interpolation nodes grows only polynomially in the number of design variables, rather than exponentially, as with naïve full-tensor interpolation. Novak and Ritter [1999], Hallatschek [1992] Our group has applied sparse polynomial interpolation to reaction-path following, Nance et al. [2014] intersystem

crossing, Nance et al. [2015] and NVE<sup>1</sup> and NVT<sup>2</sup> molecular dynamics (MD) simulations. Liu et al. [2019] Furthermore, this MD simulation framework uses classical Hamiltonian dynamics and sparse polynomial surrogate PESs to simulate the time evolution of the design variables only. Liu et al. [2019]

However, as we previously observed, the gradient of the surrogate PES is not periodic when using an all-polynomial approximation basis, even when crossing the boundary of periodic design variables (e.g., full rotations of torsion angles). This leads to nonphysical phenomena, such as nonconservation of total energy. To remedy this limitation, we constructed surrogate PESs with sparse trigonometric interpolationHallatschek [1992], Morrow and Stoyanov [2020], Griebel and Hamaekers [2014] on a tungsten molecule where the design variables are all periodic. Morrow et al. [2019] The interpolation basis functions in this case are sines and cosines. This method enforces periodicity to numerical tolerances and also produces a slightly more accurate surrogate PES than sparse polynomial interpolation on the same system. Morrow et al. [2019]

A limitation of existing interpolative PES approximation methods is that the same class of basis functions must be applied to each design variable. Nance and Kelley [2015], Morrow and Stoyanov [2020] However, many chemical systems of interest involve both periodic coordinates (e.g., full-rotation torsion angles) and nonperiodic coordinates (e.g., bond lengths, bond angles). In these systems, polynomial interpolation on periodic coordinates will lead to nonphysical phenomena due to the lack of periodicity in the surrogate PES gradient. However, trigonometric interpolation on nonperiodic coordinates will lead to persistent inaccuracies at the domain boundary called *Gibbs effects*. Helmberg [1994]

We chose azomethane for testing a new mixed-basis interpolation method. Azomethane is a relatively small molecule (N = 10 atoms), but it has interesting chemical properties to simulate. It has two stable conformers in the singlet ground state (denoted  $S_0$ ), which are *trans* and *cis*, and it is known to decompose into  $N_2$  and two methyl radicals by step-

<sup>&</sup>lt;sup>1</sup>Conserves number of particles in the system (N), volume (V), and energy (E).

<sup>&</sup>lt;sup>2</sup>Like above, but temperature (T) instead of energy.

wise dissociation after excitation to the first singlet excited state  $(S_1)$  in gas phase (Figure 1).Burton and Weisman [1990], Andrews et al. [1992] ExperimentalDiau and Zewail [2003] and ab initioSellner et al. [2010], Cattaneo and Persico [2001], Gaenko et al. [2014] studies have determined that the lifetime of azomethane in the  $S_1$  state is between 70–500 fs. Liu et al investigated the dissociation mechanism with state-average complete active space selfconsistent-field (saCASSCF) and multireference configuration interaction with single and double excitation (MRCISD) methods to prove that dissociation of the C-N bond is sequential. Liu et al. [1996] This was further studied by Sellner and coworkers using nonadiabatic ab initio surface-hopping dynamics with MCSCF-GVB-CAS and MRCISD methods. Sellner et al. [2010] Azomethane dynamics in solution are also studied with QM/MM to show that C-N dissociation is suppressed with the presence of polar or nonpolar solvents. Ruckenbauer et al. [2010] Cattaneo et al constructed a PES of azomethane at the CASSCF level and used trajectory surface hopping (TSH) and molecular dynamics surface hopping (MDSH) to show similar results. Cattaneo and Persico [2001, 2000] While we are focusing on the construction of and dynamics on the mixed-basis surrogate  $S_0$  PES of azomethane in this work, a mixedbasis PES for azomethane will be used for a reduced-dimensional TSH photoexcitation and photodissociation simulation in the future. Preliminary results indicate that when evaluating the ground-state PES with closed-shell wavefunctions, our method is able to capture conical intersections and regions of strong nonadiabatic coupling to sufficient accuracy to reproduce experimental results.

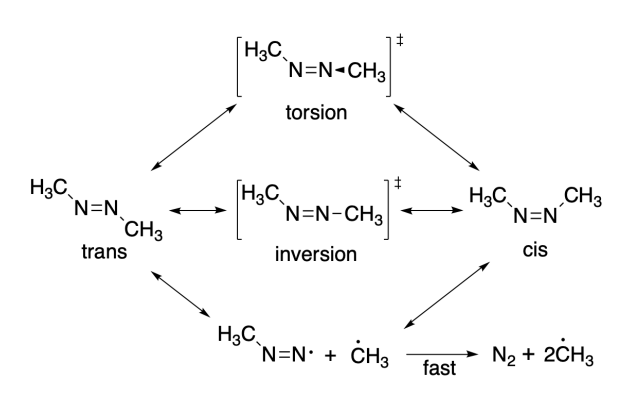


Figure 1: Isomerization and dissociation scheme of azomethane.

In this paper, we present a mixed-basis interpolative method that uses the Smolyak sparse grid construction. This method applies trigonometric interpolation to the periodic design variables and polynomial interpolation to all others. We construct a mixed-basis surrogate PES for azomethane and use it to drive a reduced-dimensional MD simulation of azomethane isomerization paths. This method requires fewer electronic structure evaluations than all-polynomial interpolation to obtain realistic energy barriers and locations of minima and transition states. Furthermore, we demonstrate explicitly that the mixed-basis surrogate appropriately conserves total energy over the entire time integration, while the all-polynomial surrogate does not.

## 2 Methods

In this section, we discuss how to construct a mixed-basis surrogate potential energy surface (PES), as well as describe the reduced-dimensional molecular dynamics (MD) framework. The full PES  $\mathcal{E}(\boldsymbol{x})$  of an N-atom molecule is a function of the internal coordinates  $\boldsymbol{x} \in \mathbb{R}^{3N-6}$ . We first partition  $\boldsymbol{x} = (\boldsymbol{q}, \boldsymbol{\xi})$ , where  $\boldsymbol{q} \in \mathbb{R}^d$  are the design variables and  $\boldsymbol{\xi}$  are the remainder variables. Then we minimize over  $\boldsymbol{\xi}$  to compute the relaxed PES:

$$E(\mathbf{q}) = \min_{\boldsymbol{\xi}} \mathcal{E}(\mathbf{q}, \boldsymbol{\xi}). \tag{1}$$

Recently there have been studies on automatically detecting the relevant design variables, Hare et al. [2019], Schmitz et al. [2020] but one often selects the design variables based on a priori chemical knowledge or empirical studies of the system. Additionally, the full Cartesian geometry of the molecule must be differentiable with respect to q, which will be discussed in Section 2.2. If a certain remainder variable has discontinuities that cannot be smoothed out, then that variable may be added to the design variables to enforce continuity. Based on continuity requirements and previous studies of azomethane, Cattaneo and Persico [2001, 2000, 1998] we chose the design variables shown in Figure 2. Three of the controlled geomet-

ric parameters  $(q_1, q_4, q_5)$  were chosen to illustrate three pathways for structural transition between *trans* and *cis*: rotation, inversion and methyl dissociation. The two methyl rotations  $(q_2, q_3)$  were controlled to prevent hydrogen atoms from unpredictably permuting their ordering during structure optimization. We describe  $\mathbf{q}$  in much greater detail in Section 3.2.

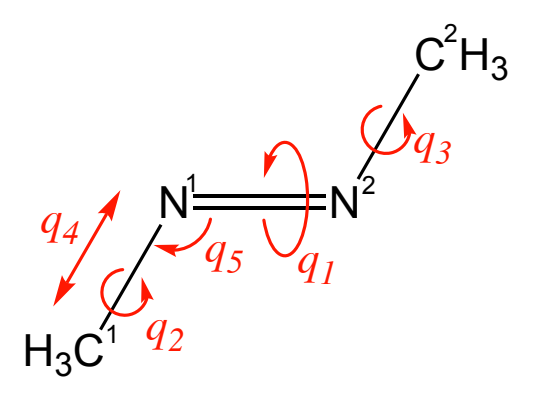


Figure 2: Structure of azomethane and design variables q.

Equation (1) requires an optimization over  $\xi$ , in addition to an approximate solution of the Schrödinger equation for  $\mathbf{q} = (\mathbf{x}, \boldsymbol{\xi})$  at each optimization step. Due to the computational cost, directly evaluating (1) repeatedly (e.g., in a dynamics simulation) is highly impractical for molecules with N > 10, rendering a surrogate model  $V(\mathbf{q}) = E^{s}(\mathbf{q})$  necessary. Compared to least-squares, an advantage of interpolatory surrogates is that, in general, fewer evaluations of the true function are necessary to achieve a given accuracy threshold. Sparse interpolation is an attractive choice because of the improved ratio of approximation accuracy to the number of interpolation nodes, leading to a more accurate surrogate with respect to the number of expensive *ab initio* calculations. Each *ab initio* calculation is independent of the others, and therefore populating the nodes is naturally parallelizable.

Previously, sparse polynomial and trigonometric interpolation have been used to construct  $E^{s}(q)$ , where one chooses the interpolation basis at the front end and applies it to each component of q. In this work, however, we aim to apply trigonometric interpolation to the periodic coordinates and polynomial interpolation to everything else. We will now provide an overview of the general sparse grid framework, as well as our mixed-basis formulation.

### 2.1 Mixed-basis formulation

Given a target function f, the general form of a sparse interpolant in both the trigonometric and polynomial case is Morrow and Stoyanov [2020], Stoyanov [2015], Stoyanov and Webster [2016]

$$G_{\Theta}[f](\boldsymbol{q}) = \sum_{i \in \Theta} t_i \, \mathcal{U}^i[f](\boldsymbol{q}), \qquad (2)$$

$$\mathcal{U}^{i}[f](q) = \sum_{j_{1}=1}^{m(i_{1})} \cdots \sum_{j_{d}=1}^{m(i_{d})} c_{j}^{i} \prod_{k=1}^{d} \phi_{j_{k}}(q_{k}).$$
(3)

In Equation (2),  $i \in \mathbb{N}_0^d$  is a multi-index,<sup>3</sup>  $\Theta = \Theta(d, L, \alpha)$  is the set of admissible multiindices, and  $t_i$  are Smolyak coefficients that depend on  $\Theta$ . In Equation (3),  $\mathcal{U}^i$  is a fulltensor interpolation operator,  $m(i_k)$  is the number of nodes along dimension k,  $c_j^i$  are the interpolation coefficients, and  $\phi_{j_k}$  are one-dimensional basis functions. The set  $\Theta$  controls the accuracy of the surrogate and is chosen to capture only the most dominant modes of the target function f. The parameter d is the number of design variables, L is the level of the sparse grid, and  $\alpha$  is an anisotropy vector, which tells  $\Theta$  which directions to favor when adding nodes. The coefficients  $t_i$  are chosen to ensure that  $G_{\Theta}[f]$  truly matches f at the interpolation nodes. The full mathematical details of this construction can be found in the Supporting Information, but we want to highlight a few important points.

First, the sparse grid is completely determined by  $\Theta$ , d, L,  $\alpha$ , and the one-dimensional interpolation rule (i.e., polynomial or trigonometric interpolation). For polynomial interpolation, we take the basis functions  $\phi_{j_k}$  to be Lagrange polynomials whose roots are the Clenshaw–Curtis points, Clenshaw and Curtis [1960] which are similar to Chebyshev nodes but nested in the interpolation level; for trigonometric interpolation, the  $\phi_{j_k}$  are sines and cosines.

Second, we are absolutely free to choose a different  $\Theta$ , d, L,  $\alpha$ , and interpolation rule

<sup>&</sup>lt;sup>3</sup>In the literature, i is sometimes called a *tensor* since it controls the size of the corresponding full-tensor grid. Morrow and Stoyanov [2020], Stoyanov and Webster [2016]

between the periodic and nonperiodic design variables.

Third, if the one-dimensional rule is nested with respect to L, then the nodes of a sparse grid are nested with respect L as well. This is critical to produce an actual interpolant and to obtain a favorable ratio of approximation error to the number of nodes. Morrow and Stoyanov [2020], Stoyanov and Webster [2016] If we refine the grid from L to L+1, then we need only to evaluate Equation (1) for the new nodes. With a nested rule, the number of nodes grows as  $\mathcal{O}(d^L)$  for d sufficiently large, Novak and Ritter [1999], Hallatschek [1992] rather than exponentially as with full-tensor interpolation. Both the Clenshaw–Curtis and trigonometric interpolation rules are nested.

Fourth, there are tools that do the heavy lifting of sparse grids, so there is no need to write one's own sparse grid code. We use the Tasmanian package from Oak Ridge National Laboratory, to which one of the authors is a contributor. Tasmanian is written in C++ with wrappers for Python, MATLAB, and Fortran, and its capabilities include (but are not limited to) both trigonometric and polynomial interpolation. Stoyanov [2015], Stoyanov et al. [2013]

The question still remains as to how we combine sparse trigonometric interpolation with sparse polynomial interpolation. The interpolation coefficients are  $c_j = f(q_j)$  for polynomial interpolation, but for trigonometric interpolation,  $c_j$  comes from a discrete Fourier transform, so we need to express Equations (2)-(3) differently. Helpfully, we may rewrite Equation (2) in adjoint formStoyanov [2015] as

$$G_{\Theta}[f](\boldsymbol{q}) = \sum_{\boldsymbol{j} \in \Theta_m} \psi_{\boldsymbol{j}}(\boldsymbol{q}) f(\boldsymbol{q}_{\boldsymbol{j}}),$$

$$\Theta_m = \bigcup_{\boldsymbol{i} \in \Theta} \left\{ \boldsymbol{j} \in \mathbb{N}^d \mid 1 \le j_k \le m(i_k), \quad \forall 1 \le k \le d \right\},$$

$$(4)$$

where  $\Theta_m$  is the set of all sparse-grid indices (as opposed to the allowable tensors i),  $\psi_j(q)$  is the adjoint basis at an evaluation point q, and  $f(q_j)$  is the function value at a specific node.

Now we partition the geometry into q = (y, z), where y contains the periodic design

variables and z has the nonperiodic ones. Furthermore, let us assume that the periodic and nonperiodic portions of f can be separated with multiplication and addition, but not function composition. This assumption is motivated by the standard separation of variables ansatz. In this case, f has the structure

$$f(\boldsymbol{q}) = f_1(\boldsymbol{y}) \otimes f_2(\boldsymbol{z}),$$

where  $f_1$  is the periodic portion of f,  $f_2$  is the nonperiodic portion, and  $\otimes$  denotes the possibility of both products and sums. Then we may use Equation (4) to apply Clenshaw–Curtis and trigonometric interpolation separately:

$$G_{\Theta}[f](\boldsymbol{q}) = \sum_{\boldsymbol{j} \in \Theta_m^{\text{trig}}} \sum_{\boldsymbol{k} \in \Theta_m^{\text{poly}}} \psi_{\boldsymbol{j}}^{\text{trig}}(\boldsymbol{y}) \psi_{\boldsymbol{k}}^{\text{poly}}(\boldsymbol{z}) f(\boldsymbol{y_j}, \boldsymbol{z_k})$$
 (5)

Equation (5) requires two grids: a sparse trigonometric grid for the periodic coordinates and a sparse polynomial-basis grid for the nonperiodic coordinates. Then, the overall grid is the tensor product of these two sparse grids. Moreover, one may think of the resulting grid as a sparse grid itself, with its own  $\Theta = \Theta^{\text{poly}} \otimes \Theta^{\text{trig}}$ . In Figure 3, we show the constituent sparse grids that we utilized in this work.

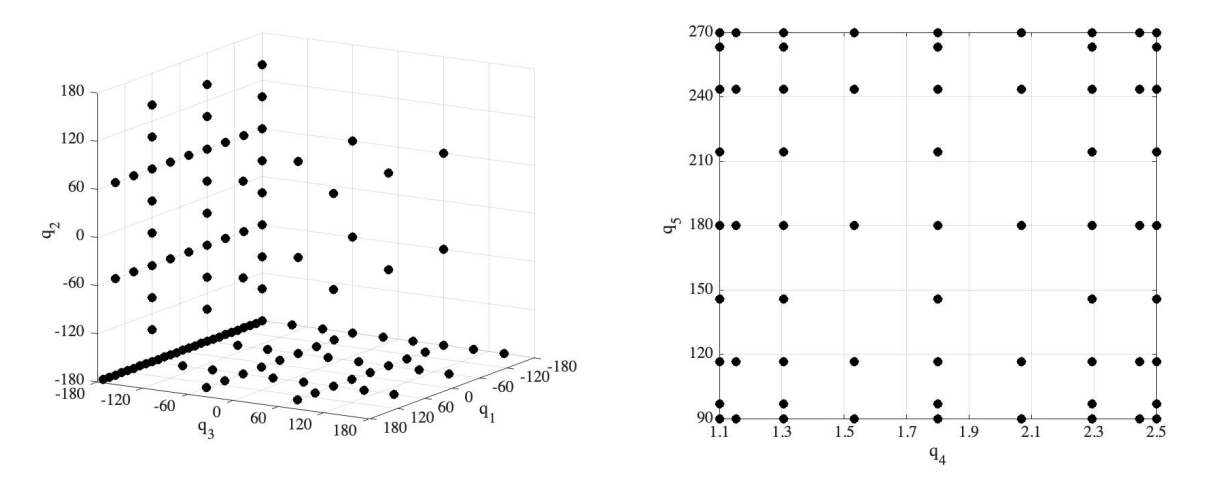


Figure 3: 7215 mixed basis nodes composed of 111 trigonometric nodes (left) and 65 polynomial nodes (right).

#### 2.2 Reduced-dimensional molecular dynamics

We follow the relaxed reduced-dimensional molecular dynamics framework originally developed by Liu and coworkers, Liu et al. [2019] which we briefly summarize here. Specifically, we use the NVE ensemble and Langevin thermostat to demonstrate the flexibility of our method. One difference between Liu's work and this work is that we have implemented our MD code in Python since Tasmanian's Python interface is much faster than its MATLAB interface. The codes, including examples, are freely available on GitHub.<sup>4</sup>

In the Hamiltonian formalism, Deriglazov [2016], Lanczos [2012] the equations of motion for the design variables  $\boldsymbol{q}$  and the generalized momenta  $\boldsymbol{p}$  are

$$\begin{cases} \dot{q} = \frac{\partial \mathcal{H}}{\partial \mathbf{p}} \\ \dot{\mathbf{p}} = -\frac{\partial \mathcal{H}}{\partial \mathbf{q}} \end{cases}$$
 (6)

The classical Hamiltonian is a sum of potential and kinetic energy terms, expressed as

$$\mathcal{H}(\boldsymbol{q}, \boldsymbol{p}) = V(\boldsymbol{q}) + K(\boldsymbol{q}, \boldsymbol{p}) \tag{7}$$

where V(q) is the sparse interpolant of the relaxed PES and K(q, p) involves the momenta and Wilson's G-matrix:Wilson et al. [1955]

$$K(\boldsymbol{q}, \boldsymbol{p}) = \frac{1}{2} \boldsymbol{p}^T \boldsymbol{G}^{-1}(\boldsymbol{q}) \boldsymbol{p}, \tag{8}$$

$$G_{ij}(\mathbf{q}) = \sum_{k=1}^{3N} m_k \frac{\partial X_k(\mathbf{q})}{\partial q_i} \frac{\partial X_k(\mathbf{q})}{\partial q_j}$$
(9)

The function  $X : \mathbb{R}^d \to \mathbb{R}^{3N}$  maps the design variables to the full Cartesian molecular geometry, and  $m_k$  is the atomic mass corresponding to Cartesian component  $X_k$ . In order to conserve energy and be approximated with sparse interpolation, X(q) must be differentiable,

<sup>&</sup>lt;sup>4</sup> https://github.com/zbmorrow/mixed\_basis\_rrmd

including across periodic boundaries.

To integrate the system forward in time, we must first choose  $q(0) = q_0$  and compute  $p(0) = p_0$ . The momenta are computed by selecting a starting temperature T and drawing 3N Cartesian velocities from a Boltzmann distribution

$$\mathbf{v}_0 = \sqrt{k_B \, \mathbf{M}^{-1} \, T} \, \mathbf{R}_t \,, \qquad \mathbf{R}_t \sim \mathcal{N}(\mathbf{0}, \mathbf{I}).$$
 (10)

Here,  $k_B$  is the Boltzmann constant in appropriate units,  $\mathbf{M} = \text{diag}(m_1, \dots, m_{3N})$ , and  $\mathbf{R}_t$  is a 3N-dimensional standard normal random variable realized at time t. We then project the initial velocities onto the reduced-dimensional space by setting

$$p(0) = \mathbf{X}'(\mathbf{q}_0)^T \mathbf{v}_0, \qquad (\mathbf{X}'(\mathbf{q}))_{ij} = \frac{\partial X_i(\mathbf{q})}{\partial q_i}.$$
 (11)

From Equations (7)–(9), we need to construct a surrogate PES V(q) and Cartesian mapping function X(q), which we approximate using sparse interpolation.

#### 2.2.1 NVE simulations

In the NVE ensemble, we wish to simulate the trajectory of a molecule while conserving total energy. We integrate the system forward in time with the Störmer-Verlet method, which conserves total energy. Verlet [1967], Störmer [1912] At step  $t = t_n$ , the system is propagated forward by the three-step process

$$\begin{cases}
\mathbf{q}_{n+1/2} &= \mathbf{q}_n + \frac{\Delta t}{2} \frac{\partial \mathcal{H}(\mathbf{q}_{n+1/2}, \mathbf{p}_n)}{\partial \mathbf{p}} \\
\mathbf{p}_{n+1} &= \mathbf{p}_n - \frac{\Delta t}{2} \left[ \frac{\partial \mathcal{H}(\mathbf{q}_{n+1/2}, \mathbf{p}_n)}{\partial \mathbf{q}} + \frac{\partial \mathcal{H}(\mathbf{q}_{n+1/2}, \mathbf{p}_{n+1})}{\partial \mathbf{q}} \right] \\
\mathbf{q}_{n+1} &= \mathbf{q}_{n+1/2} + \frac{\Delta t}{2} \frac{\partial \mathcal{H}(\mathbf{q}_{n+1/2}, \mathbf{p}_{n+1})}{\partial \mathbf{p}}
\end{cases}$$
(12)

The first step is an implicit Euler half-step in q, the second is a full Crank-Nicolson step in p, and the third is an explicit Euler half-step in q.Gautschi [2012] The derivatives are

expressed as

$$\frac{\partial \mathcal{H}}{\partial \boldsymbol{q}} = \frac{\partial V}{\partial \boldsymbol{q}} + \frac{\partial K}{\partial \boldsymbol{q}} \tag{13}$$

$$\frac{\partial \mathcal{H}}{\partial \boldsymbol{p}} = \boldsymbol{G}^{-1}(\boldsymbol{q})\,\boldsymbol{p} \tag{14}$$

and then evaluated numerically. The first two steps of Störmer–Verlet involve solving a nonlinear system of equations. For the all-polynomial surrogates, we use a derivative-free optimizer in the SciPy packageVirtanen et al. [2020], Powell [1964] since polynomial gradients are not guaranteed to be continuous across the periodic boundary. Morrow et al. [2019] Such derivative-free methods are more computationally costly, but they are the only option for regions near the periodic boundary, where the surrogates are not differentiable. An advantage of the mixed-basis method is that we may solve the nonlinear system with Newton's method, Kelley [1995, 2018] which is much cheaper computationally, since the surrogates are differentiable across the periodic boundary.

#### 2.2.2 Langevin thermostat

The Langevin thermostat is a very popular algorithm for NVT simulations, in which temperature is conserved. The equations of motion (6) become a system of stochastic differential equations with additional terms to incorporate the coupling between the system and a thermal bath. Allen and Tildesley [2017] In Cartesian coordinates (Q, P), the Langevin equations are

$$\begin{cases} d\mathbf{Q} = \frac{\partial \mathcal{H}}{\partial \mathbf{P}} dt \\ d\mathbf{P} = -\frac{\partial \mathcal{H}}{\partial \mathbf{Q}} dt - \gamma \mathbf{P} dt + \boldsymbol{\sigma} d\mathbf{w} \end{cases}$$
(15)

where Q and P are the position and momentum of the particle. The additional terms capture the viscosity of the bath  $(-\gamma P)$  and random forces  $(\sigma dw)$ , without which (15) and (6) are equivalent. From the fluctuation-dissipation theorem, the coefficient  $\sigma_i$  can be written in terms of  $\gamma$  as

$$\sigma_i = \sqrt{2\gamma m_i k_B T} \tag{16}$$

where T is the target temperature. Allen and Tildesley [2017], Leimkuhler and Matthews [2013] Like Liu and coworkers, Liu et al. [2019] we employ the BAOAB method of Leimkuhler and Matthews Leimkuhler and Matthews [2013,?] to integrate (15). In the reaction coordinates (q, p), the BAOAB method is

(BA) 
$$\begin{cases} \boldsymbol{p}_{n+1/2} &= \boldsymbol{p}_{n} - \frac{\Delta t}{2} \frac{\partial \mathcal{H}(\boldsymbol{q}_{n}, \boldsymbol{p}_{n+1/2})}{\partial \boldsymbol{q}} \\ \boldsymbol{q}_{n+1/2} &= \boldsymbol{q}_{n} + \frac{\Delta t}{2} \frac{\partial \mathcal{H}(\boldsymbol{q}_{n}, \boldsymbol{p}_{n+1/2})}{\partial \boldsymbol{p}} \end{cases},$$
(17)

(O) 
$$\left\{ \boldsymbol{p}_{n+1/2}' = e^{-\gamma \Delta t} \boldsymbol{p}_{n+1/2} + \sqrt{1 - e^{-2\gamma \Delta t}} \, \boldsymbol{X}' (\boldsymbol{q}_{n+1/2})^T \sqrt{k_B \boldsymbol{M} T} \, \boldsymbol{R}_t \right., \tag{18}$$

(AB) 
$$\begin{cases} \boldsymbol{q}_{n+1} &= \boldsymbol{q}_{n+1/2} + \frac{\Delta t}{2} \frac{\partial \mathcal{H}(\boldsymbol{q}_{n+1}, \boldsymbol{p}'_{n+1/2})}{\partial \boldsymbol{p}} \\ \boldsymbol{p}_{n+1} &= \boldsymbol{p}'_{n+1/2} - \frac{\Delta t}{2} \frac{\partial \mathcal{H}(\boldsymbol{q}_{n+1}, \boldsymbol{p}'_{n+1/2})}{\partial \boldsymbol{q}} \end{cases}$$
(19)

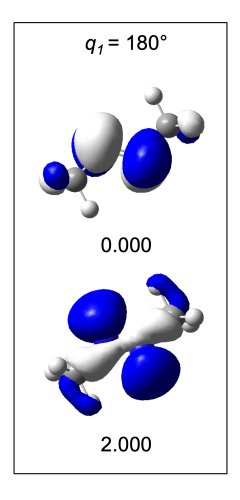
## 3 Results and Discussion

We used our mixed-basis formulation to construct surrogates for the  $S_0$  PES and the Cartesian mapping function X(q). In an NVE framework, we compared the performance of the mixed-basis surrogate to both on-the-fly full-dimensional Born-Oppenheimer molecular dynamics (BOMD)Helgaker et al. [1990], Uggerud and Helgaker [1992] and the previous state of the art, which uses an all-polynomial interpolation basis. Liu et al. [2019] We then use a Langevin thermostat to demonstrate that our mixed-basis surrogate produces accurate temperature distributions and that azomethane isomerization is not likely to occur on the  $S_0$  surface alone, even at high temperatures.

#### 3.1 Electronic structure of azomethane

All electronic structure calculations utilized the Gaussian 16 software packageFrisch et al. [2016] with the B3LYP hybrid functionalBecke [1993,?], Lee et al. [1988], Stephens et al. [1994] and the 6-311G\* basis set.Krishnan et al. [1980] The computing environment was Henry2, a high-performance computing cluster at North Carolina State University. Each Gaussian instance used 16 cores on an Intel Xeon processor and was allocated 32GB RAM. Further details on the electronic structure calculations are in Section 3.2 and the Supporting Information.

One of the chemical properties of azomethane that is important to note is that its lowestenergy electronic state depends on the C-N=N-C dihedral rotation. As illustrated by the natural orbitals in Figure 4, the nitrogen lone-pair orbital and  $\pi^*$  of nitrogen 2p orbitals become degenerate in the ground state of azomethane when  $q_1 = 90^{\circ}$ . Therefore, when the PES is calculated with closed-shell restricted wavefunctions, we observe a sharp peak near  $q_1 = 90^{\circ}$ . In order to obtain a smooth PES, the stability testsBauernschmitt and Ahlrichs [1996] of DFT wavefunctions were performed after each calculation.



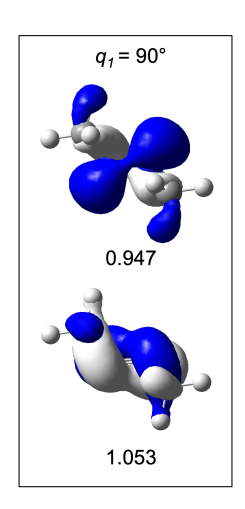


Figure 4: Natural orbitals of azomethane for  $q_1 = 180^{\circ}$  and  $q_1 = 90^{\circ}$  at isovalue of 0.02  $e^{1/2} \,(\text{bohr})^{-3/2}$ , where e denotes the charge of an electron, with occupation numbers. The colors represent positive (blue) and negative (light grey) phases of the wavefunction.

#### 3.2 Constructing the surrogate PES

Each geometry is supplied to Gaussian in Cartesian coordinates, but the optimization uses redundant internal coordinates. Each Gaussian job proceeds as follows: (1) stability check-Bauernschmitt and Ahlrichs [1996] on wavefunction, (2) optimizationLi and Frisch [2006] over remainder variables, (3) stability check, (4) optimization and frequency analysis, and (5) stability check. The safeguards are to ensure that the relaxation over  $\boldsymbol{\xi}$  found a true minimum and that the lowest-energy wavefunction is selected. In this way, we can build surrogates for  $E_{S_0}(\boldsymbol{q})$  and  $\boldsymbol{X}_{S_0}(\boldsymbol{q})$ . We provide sample Gaussian input files in the Supporting Information.

The design variables, shown in Figure 2, are defined as follows:

- 1.  $q_1 \in [-180, 180]$  is the C<sup>1</sup>-N<sup>1</sup>=N<sup>2</sup>-C<sup>2</sup> dihedral angle;
- 2.  $q_2 \in [-180, 180]$  is equal to the N<sup>2</sup>=N<sup>1</sup>-C<sup>1</sup>-H dihedral angle plus  $(q_1 + 180)$ , which we will explain shortly;
- 3.  $q_3 \in [-180, 180]$  is the N<sup>1</sup>=N<sup>2</sup>-C<sup>2</sup>-H' dihedral angle;
- 4.  $q_4 \in [1.1, 2.5]$  is the N<sup>1</sup>-C<sup>1</sup> bond length; and
- 5.  $q_5 \in [90, 270]$  is the  $N^2 = N^1 C^1$  bond angle.

Angles are measured in degrees, and bond lengths in Å. The variables  $q_1$ ,  $q_2$ , and  $q_3$  are periodic, while  $q_4$  and  $q_5$  are nonperiodic. We do not freeze the other C–N distance or N=N-C bond angle during geometry optimizations; scans along these parameters have a single minimum which produced a continuous surface. Our aim is to study azomethane photodynamics, and since the stepwise dissociation mechanism has been established in prior work, we simply terminate the simulation when one C–N bond is broken. We allow  $q_5$  to be linear or greater than 180° in order to capture methyl inversion, in accordance with previous work. Cattaneo and Persico [2001, 1998] The lower bound on  $q_4$  and both bounds on  $q_5$  were chosen to be the widest possible bounds without the molecule dissociating during

the optimization process. We need a large enough domain on either side of the equilibrium  $q_5$  value to capture the well. Furthermore, the PES is mostly flat in the  $q_4$  direction for  $q_4 > 2.5$ , Cattaneo and Persico [2001] so we truncated the domain to ensure that X(q) is smooth; if  $q_4$  drifts beyond 2.5 Å during the course of an MD simulation, we consider the molecule dissociated and terminate the simulation. The design variable  $q_2$  was originally not part of our set of design variables but was added to maintain continuity of X(q).

Since the energy of a molecule is invariant with respect to translations or rotations of the entire system, we must reconstruct the Cartesian geometries at the nodes in a consistent manner in order to build X(q). Liu, Jakubikova, and Kelley used Kabsch alignment to minimize the root-mean-squared deviation between each node and the global minimum. However, their application was NH<sub>3</sub> inversion, in which all atoms except nitrogen are moving confluently; in our system, several atoms (e.g. N<sup>1</sup>, N<sup>2</sup>, C<sup>2</sup>) are mostly stationary. To obtain consistent Cartesian geometries, we apply translations and rotations of the entire molecule to place N<sup>1</sup> at the origin, N<sup>2</sup> on the positive x-axis, and C<sup>2</sup> in Quadrant I of the xy-plane. We then load these geometries into Tasmanian to construct X(q).

Since the molecule can be linear or  $q_5 > 180$  and since the Cartesian mapping function X(q) must be smooth, we need to take special care to encode the geometry properly in our input files. For a given sparse grid node  $q^i$ , we apply the following transformations before converting from internal coordinates to Cartesian:

- 1. If  $q_5^i > 180$ , then we set  $q_1^i \leftarrow 180 + q_1^i, \ q_2^i \leftarrow 180 + q_2^i, \ \text{and} \ q_5^i \leftarrow 360 q_5^i$ .
- 2. After Step 1, if  $q_5^i < 180$ , we recover the N<sup>2</sup>=N<sup>1</sup>-C<sup>1</sup>-H dihedral by setting  $q_2^i \leftarrow q_2^i (q_1^i + 180)$ . This step is necessary to avoid multivalued geometries in the limit  $q_5 \rightarrow 180$ . See the animations in the Supporting Information to view the effect on the methyl group.

After finishing one batch sparse grid nodes, we examine the surrogate PESs by plotting various 2-D slices and optimizing the geometry on the surface to a local minimum or transition state. We also animated 50 randomly generated one-dimensional trajectories by restricting all but one design variable. We are able to examine slices to detect inaccuracies since the interpolation basis functions are global rather than local. We refine the sparse grid until (a) the calculated energies, relative to the *trans*- minimum, are within  $\sim$ 5% of their Gaussian-optimized value and (b) all animations are smoothly varying. We show two representative slices near the global minimum in Figure 5. The Supporting Information (Table S2) shows the energies and geometries at minima and saddle points for the highest level of refinement, as well as a selection of animations of X(q).

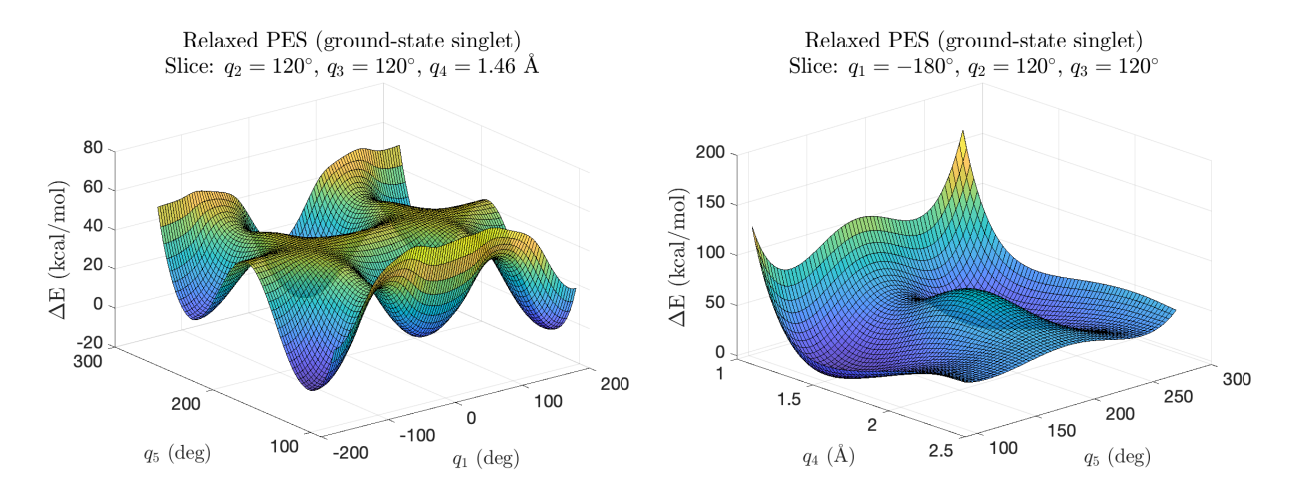


Figure 5: Mixed-basis surrogate PESs for the singlet ground state.

## 3.3 NVE: Mixed vs. all-polynomial basis

We begin by subjecting the surrogates to a relatively easy test: an NVE simulation at the trans- minimum on the  $S_0$  surface.Liu et al. [2019] We will compare full-dimensional on-the-fly BOMD, a mixed-basis surrogate, and an all-polynomial surrogate. Table 1 shows the initial geometry used for each flavor of surrogate. Ten initial velocities  $\mathbf{v}(0) \in \mathbb{R}^{3N}$  are drawn from a Boltzmann distribution at 298.15 Kelvin. These are immediately used to run on-the-fly BOMD in Gaussian 16. For reduced-dimensional MD, we project the initial velocities onto  $\mathbf{p}(0)$  using the surrogate  $\mathbf{X}(\mathbf{q})$  corresponding to the basis in use. We integrate up to 2.5 ps with step size  $\Delta t = 0.1$  fs.

Table 1: Minimizers for the trans- conformer.

	# nodes	argmin $(q_1, q_2, q_3, q_4, q_5)$
Gaussian		[180.00, 122.20, 122.20, 1.46, 113.00]
Mixed basis	7215	[-179.71, 121.91, 121.84, 1.46, 116.06]
All polynomial	17233	[-179.63, 137.91, -155.80, 1.47, 113.16]

When measuring energy conservation in an MD simulation, one first stores kinetic and total energy at each time step. Then, the general heuristic is to want

$$\frac{\sigma(\lbrace K_i + V_i \rbrace)}{\sigma(\lbrace K_i \rbrace)} \le \mathcal{O}(10^{-4}) \tag{20}$$

where  $\sigma$  denotes the standard deviation of the observations. Allen and Tildesley [2017] In this way, the variation in total energy is normalized by the variation in kinetic energy, and the heuristic threshold allows us to determine whether a method suitably conserves energy. We computed these ratios for each run and method and show the results in Table 2. Onthe-fly BOMD uses the full 24 degrees of freedom, rather than the five degrees of freedom in the reduced-dimensional surrogates, which contributes to the slightly higher conservation ratio compared to the mixed basis. Nonetheless, the sample means for BOMD and mixed-basis MD are within the usual bound, while that of the all-polynomial surrogate is orders of magnitude too large. Furthermore, the runtime is much lower when using a surrogate model, particularly for the mixed basis, which has the fastest turnaround time and lowest core usage. The core-hour usage of mixed-basis NVE MD is an order of magnitude lower than that of all-polynomial MD and two orders of magnitude lower than BOMD. In Figure 6, we show the iteration history of total energy during one of polynomial-basis simulations. When each jump occurs, at least one periodic design variables is near  $\pm 180^{\circ}$ .

In Figure 7 we show histograms for selected design variables, remainder variables, and potential energy. Table 3 shows the mean, standard deviation, and range of each histogram. We show the all-polynomial results for completeness, but we re-emphasize that the all-polynomial surrogate does not conserve total energy. The degeneracy noted in Section 3.1

Table 2: Statistics of energy conservation ratios for each method, along with performance.

	BOMD	Mixed basis	All-polynomial
Mean	$7.5 \times 10^{-4}$	$1.8 \times 10^{-5}$	$1.8 \times 10^{-1}$
Stdev	$4.0 \times 10^{-4}$	$1.2 \times 10^{-5}$	$1.0 \times 10^{-1}$
Min	$3.4 \times 10^{-4}$	$6.2 \times 10^{-6}$	$6.5 \times 10^{-2}$
Max	$1.6\times10^{-3}$	$4.5 \times 10^{-5}$	$4.1 \times 10^{-1}$
Avg wall time (hr)	41.11	0.67	7.04
Cores	16	1	5

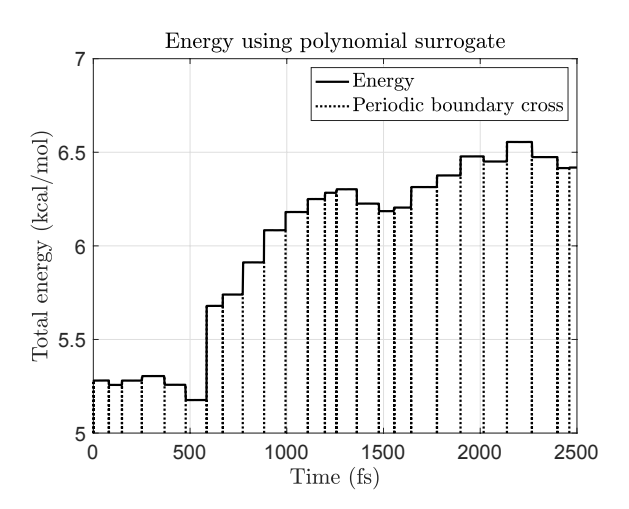


Figure 6: Solid line: total energy. Dotted lines:  $q_1,\,q_2,\,{\rm or}\,\,q_3$  is within  $0.03^\circ$  of  $\pm 180^\circ$ .

does not appear in these BOMD results since  $q_1$  never drifts outside [167.4, 192.0]. For the N=N distance, the distribution of the mixed-basis trajectory is tight around its mean value since r(N=N) was optimized out when populating the sparse grid. For the design variables, certain distributions appear to have roughly the correct shape but are shifted right or left from BOMD. This is due to the surrogate PESs having slightly different equilibrium values for the trans- minimum.

Since both reduced-dimensional surrogates use less than the full 3N-6 internal coordinates, while BOMD uses all of them, we estimate the contribution of the remainder variables  $\boldsymbol{\xi}$  in a manner analogous to Liu and coworkers. Liu et al. [2019] At time step i, we add the contributions from  $\boldsymbol{\xi}$  by setting

$$V_i^{\text{corrected}} = V_i^{\text{surrogate}} + \eta_i$$

where  $\eta_i$  is a uniform random variable on the interval  $[0, \mathcal{H}_{BOMD} - \mathcal{H}_{surrogate}]$ . Ideally, we would isolate the effects of the BOMD framework from the usage of additional design variables (i.e. by using a full-dimensional surrogate PES), but constructing the full 24-dimensional PES is computationally infeasible. As a result, the corrected distributions for V(q) in Figure 7 do not match BOMD exactly.

## 3.4 Langevin thermostat

In this section, we focus only on the mixed-basis surrogate since it has been demonstrated that a polynomial surrogate will not properly capture energy when crossing a periodic boundary. We wish to study the effect of temperature on azomethane geometry. We start at the trans- minimum on the  $S_0$  surface and integrate to 40 ps with a time step of  $\Delta t = 0.05$  fs at various target temperatures T. The time step needs to be suitably small for Newton's method to converge. We used a relatively modest value for the friction coefficient,

<sup>&</sup>lt;sup>5</sup>We determined to need  $\Delta t = 0.05$  fs for T = 3000 K, and we used it in all runs for consistency.

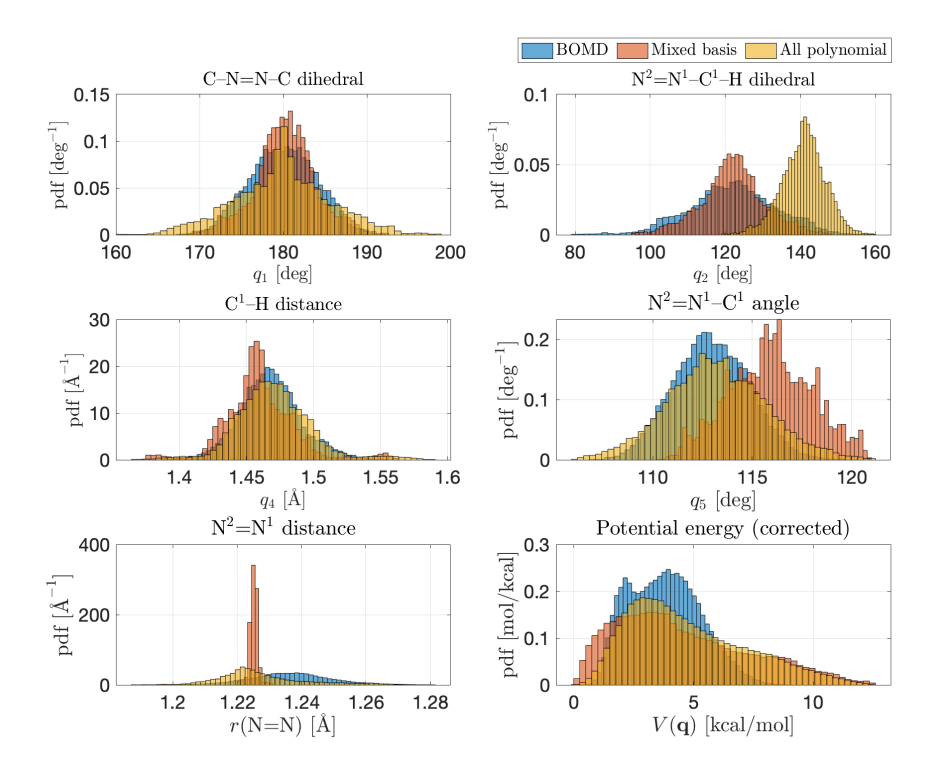


Figure 7: Histograms of selected design variables, remainder variables, and potential energy.

Table 3: Statistics from NVE MD trajectories.

		BOMD	Mixed basis	All-polynomial
$q_1 \text{ (deg)}$	mean	180.0	180.3	179.9
	stdev	4.0	3.7	5.8
	range	[167.4, 192.0]	[168.0, 192.3]	[159.3, 198.6]
$q_2 \text{ (deg)}$	mean	122.2	122.1	140.8
	stdev	11.0	8.5	5.7
	range	[77.6, 178.0]	[95.3, 147.7]	[119.5, 159.1]
q <sub>4</sub> (Å)	mean	1.47	1.46	1.47
	stdev	0.02	0.03	0.03
	range	[1.39, 1.56]	[1.37, 1.56]	[1.37, 1.59]
$q_5  ext{ (deg)}$	mean	112.9	115.9	113.2
	stdev	1.9	2.1	2.5
	range	[106.9, 119.6]	[110.4, 121.0]	[106.1, 121.2]
$r({ m N=N})~({ m \AA})$	mean	1.24	1.23	1.23
	stdev	0.013	0.001	0.013
	range	[1.19, 1.28]	[1.22, 1.23]	[1.19, 1.28]
$V(oldsymbol{q})  ext{ (kcal/mol)}$	mean	3.8	4.6	4.8
	stdev	1.5	2.8	2.4
	range	[0.00, 8.9]	[0.02, 12.56]	[0.03, 12.53]

 $\gamma = 0.01 \text{ fs}^{-1}$ . Liu et al. [2019], Cattaneo and Persico [1998] Initial velocities are drawn from a Boltzmann distribution at temperature T and then projected onto  $\mathbf{p}(0)$ .

We show the results in Figure 8. The average runtime of each thermostat simulation was 22.9 hours on XSEDE Bridges-2 with a single core. Towns et al. [2014], Nystrom et al. [2015] To demonstrate the reconstruction of the full Cartesian geometry with X(q), the Supporting Information contains an animation of the geometry evolution after thermal equilibration. Even 3000 K is not hot enough to overcome the torsion transition structure  $(q_1 \approx 90)$ . Furthermore, the dissociation energy of the  $C^1$ -N<sup>1</sup> bond is lower than the energy barrier of the torsion transition state. Cattaneo and Persico [2000] As a result, isomerization is not energetically favorable via  $S_0$  and temperature alone. In Figure 8(b), we have plotted the sample means and standard deviations of ensemble temperature versus their theoretical expectation values. Instantaneous temperature  $\mathcal{T}(q, p)$  is related to kinetic energy K(q, p) by

$$\mathcal{T}(\boldsymbol{q}, \boldsymbol{p}) = \frac{2K(\boldsymbol{q}, \boldsymbol{p})}{d k_B}$$

where d is the number of design variables. From the equipartition theorem, Münster [1969] maximum likelihood estimators for the mean and standard deviation of  $\mathcal{T}$  are given by

$$\mu(\mathcal{T}) = T$$

$$\sigma(\mathcal{T}) = \sqrt{2/d} \ T$$

where T is the target temperature of the thermostat. The theoretical and observed statistics agree closely with each other.

## 4 Conclusions

We have presented a mixed-basis interpolation algorithm that uses trigonometric interpolation on periodic design variables and polynomial interpolation on nonperiodic design vari-

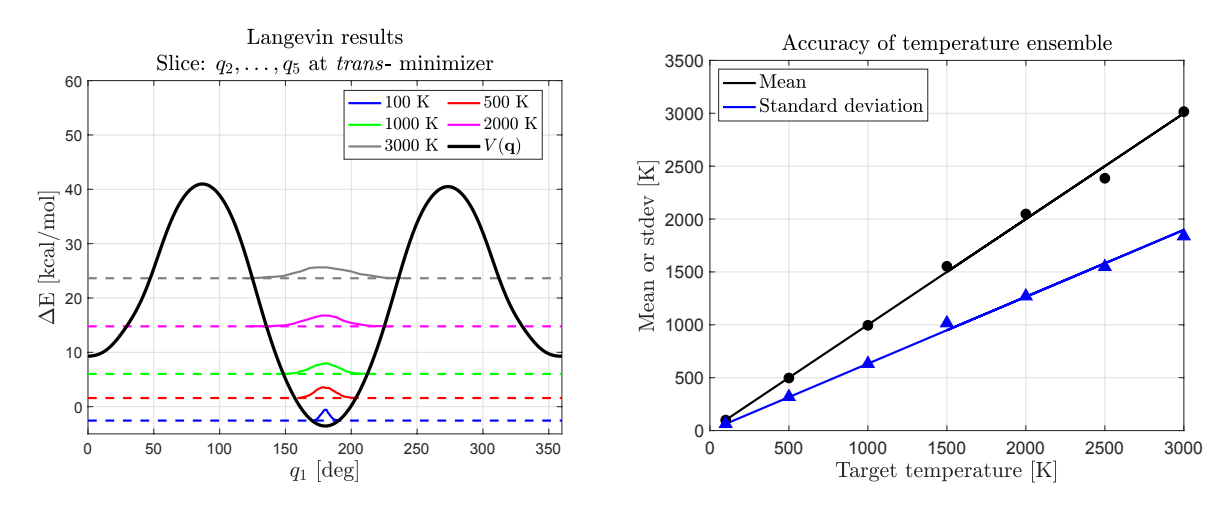


Figure 8: Left: Geometry distribution (solid) and average total energy (dashed lines) at different temperatures. Right: Predicted (lines) and observed (dots/triangles) statistical values for temperature.

ables. Unlike previous methods, it is not limited to molecules with purely periodic or purely nonperiodic reaction coordinates, and therefore is an improvement over the prior state of the art (same-basis interpolation) and widely generalizable to different systems. The results demonstrate that our method conserves total energy within accepted tolerances, is computationally efficient, and accurately reproduces the temperature distribution of a thermostat in a reduced-dimensional MD framework. The Python codes for mixed-basis interpolative PES approximation and reduced-dimensional MD are freely available on GitHub.<sup>4</sup>

This work has investigated only the lowest-lying singlet state of azomethane, but it is known that light-induced  $S_0 \to S_1$  excitation is a likely isomerization and decomposition pathway for azomethane. Sellner et al. [2010], Cattaneo and Persico [2001, 1998] An extension of our surrogate PES approximation will be to implement the fewest-switches surface hopping (FSSH) algorithm of TullyTully [1990], Nance [2015] in a reduced-dimensional setting.

## Supporting Information Available

Mathematical details of sparse interpolation and example Gaussian input files (pdf). Data for trigonometric and polynomial PESs (xlsx). Animations of selected geometry trajectories

(mp4).

## Acknowledgement

The authors gratefully acknowledge support from the National Science Foundation under Grant No. DGE-1746939 of the NSF-GRFP (Z.M.), Grant Nos. DMS-1745654 and DMS-1906446 (C.T.K.), and Grant No. CHE-1554855 (E.J and H.K.). Any opinions, findings, conclusions, or recommendations expressed in this material are those of the author(s) and do not necessarily reflect the views of the National Science Foundation.

This work used the Extreme Science and Engineering Discovery Environment (XSEDE), which is supported by National Science Foundation Grant No. ACI-1548562. Towns et al. [2014] Specifically, it used the Bridges-2 system, which is supported by NSF Grant No. ACI-1928147, at the Pittsburgh Supercomputing Center (PSC). Nystrom et al. [2015] We acknowledge the computing resources provided on Henry2, a high-performance computing cluster operated by North Carolina State University.

We would also like to thank Miroslav Stoyanov for fruitful discussions about the efficient implementation of the mixed-basis construction.

## References

Born, M.; Oppenheimer, R. Zur Quantentheorie der Molekeln. Ann. Phys. – Berlin 1927, 389, 457–484.

Born, M.; Fock, V. Beweis des Adiabatensatzes. Z. Phys. 1928, 51, 165–180.

Born, M.; Huang, K. Dynamical Theory of Crystal Lattices; Oxford University Press, 1954.

Glasstone, S.; Eyring, H.; Laidler, K. J. *The Theory of Rate Processes*; McGraw-Hill, New York, 1941.

- Albaugh, A.; Boateng, H. A.; Bradshaw, R. T.; Demerdash, O. N.; Dziedzic, J.; Mao, Y.; Margul, D. T.; Swails, J.; Zeng, Q.; Case, D. A.; Eastman, P.; Wang, L.-P.; Essex, J. W.; Head-Gordon, M.; Pande, V. S.; Ponder, J. W.; Shao, Y.; Skylaris, C.-K.; Todorov, I. T.; Tuckerman, M. E.; Head-Gordon, T. Advanced Potential Energy Surfaces for Molecular Simulation. J. Phys. Chem. B 2016, 120, 9811–9832.
- Brown, A.; Braams, B. J.; Christoffel, K.; Jin, Z.; Bowman, J. M. Classical and Quasiclassical Spectral Analysis of CH<sub>5</sub><sup>+</sup> Using an Ab Initio Potential Energy Surface. *J. Chem. Phys.* **2003**, *119*, 8790–8793.
- Bowman, J. M.; Czakó, G.; Fu, B. High-Dimensional Ab Initio Potential Energy Surfaces for Reaction Dynamics Calculations. *Phys. Chem. Chem. Phys.* **2011**, *13*, 8094–8111.
- Liu, C.; Kelley, C. T.; Jakubikova, E. Molecular Dynamics Simulations on Relaxed Reduced-Dimensional Potential Energy Surfaces. J. Phys. Chem. A 2019, 4543–4554.
- Nance, J.; Jakubikova, E.; Kelley, C. T. Reaction Path Following with Sparse Interpolation. *J. Chem. Theory Comput.* **2014**, *10*, 2942–2949.
- Koch, W.; Holthausen, M. A Chemist's Guide to Density Functional Theory, 2nd ed.; Wiley, 2001.
- Collins, M. A.; Parsons, D. F. Implications of Rotation–Inversion–Permutation Invariance for Analytic Molecular Potential Energy Surfaces. *J. Chem. Phys.* **1993**, *99*, 6756–6772.
- Collins, M. A. Molecular Potential-Energy Surfaces for Chemical Reaction Dynamics. *Theor. Chem. Acc.* **2002**, *108*, 313–324.
- Collins, M. A. Molecular Potential Energy Surfaces by Interpolation. *Lec. Notes Comput. Sci.* **2003**, 159–167.
- Thompson, K. C.; Jordan, M. J. T.; Collins, M. A. Polyatomic Molecular Potential Energy

- Surfaces by Interpolation in Local Internal Coordinates. J. Chem. Phys. 1998, 108, 8302–8316.
- Espinosa-Garcia, J.; Monge-Palacios, M.; Corchado, J. C. Constructing Potential Energy Surfaces for Polyatomic Systems: Recent Progress and New Problems. *Adv. Phys. Chem.* **2012**, 164752.
- Wu, T.; Manthe, U. A Potential Energy Surface Construction Scheme for Accurate Reaction Rate Calculations: General Approach and a Test for the H + CH<sub>4</sub> → H<sub>2</sub> + CH<sub>3</sub> Reaction. J. Chem. Phys. 2003, 119, 14–23.
- Zhou, Y.; Fu, B.; Wang, C.; Collins, M. A.; Zhang, D. H. Ab Initio Potential Energy Surface and Quantum Dynamics for the  $H + CH_4 \rightarrow H_2 + CH_3$  Reaction. J. Chem. Phys. **2011**, 134, 064323.
- Braams, B. J.; Bowman, J. M. Permutationally Invariant Potential Energy Surfaces in High Dimensionality. *Int. Rev. Phys. Chem.* **2009**, *28*, 577–606.
- Chen, Q.; Bowman, J. M. Quantum and Classical IR Spectra of (HCOOH)<sub>2</sub>, (DCOOH)<sub>2</sub> and (DCOOD)<sub>2</sub> Using Ab Initio Potential Energy and Dipole Moment Surfaces. *Faraday Discuss.* **2018**, 33–49.
- Qu, C.; Yu, Q.; Bowman, J. M. Permutationally Invariant Potential Energy Surfaces. Annu. Rev. Phys. Chem. 2018, 69, 151–175.
- Dawes, R.; Quintas-Sánchez, E. Rev. Comp. Ch.; John Wiley & Sons, Ltd, 2018; Chapter 5, pp 199–263.
- Guo, Y.; Tokmakov, I.; Thompson, D. L.; Wagner, A. F.; Minkoff, M. Interpolating Moving Least-Squares Methods for Fitting Potential Energy Surfaces: Improving Efficiency via Local Approximants. J. Chem. Phys. 2007, 127, 214106.
- McLain, D. H. Drawing Contours from Arbitrary Data Points. Comput. J. 1974, 17, 318–324.

- Farwig, R. Rate of Convergence of Shepard's Global Interpolation Formula. *Math. Comput.* **1986**, *46*, 577–590.
- Maisuradze, G. G.; Thompson, D. L.; Wagner, A. F.; Minkoff, M. Interpolating Moving Least-Squares Methods for Fitting Potential Energy Surfaces: Detailed Analysis of Onedimensional Applications. J. Chem. Phys. 2003, 119, 10002–10014.
- Cui, J.; Krems, R. V. Gaussian Process Model for Collision Dynamics of Complex Molecules. Phys. Rev. Lett. 2015, 115, 073202.
- Uteva, E.; Graham, R. S.; Wilkinson, R. D.; Wheatley, R. J. Interpolation of Intermolecular Potentials Using Gaussian Processes. *J. Chem. Phys.* **2017**, *147*, 161706.
- Jiang, B.; Li, J.; Guo, H. Potential Energy Surfaces from High Fidelity Fitting of Ab Initio Points: The Permutation Invariant Polynomial—Neural Network Approach. Int. Rev. Phys. Chem. 2016, 35, 479–506.
- Lorenz, S.; Groß, A.; Scheffler, M. Representing High-Dimensional Potential-Energy Surfaces for Reactions at Surfaces by Neural Networks. *Chem. Phys. Lett.* **2004**, *395*, 210–215.
- Manzhos, S.; Dawes, R.; Carrington, T. Neural Network-Based Approaches for Building High Dimensional and Quantum Dynamics-Friendly Potential Energy Surfaces. *Int. J. Quantum Chem.* **2014**, *115*, 1012–1020.
- Lin, Q.; Zhang, L.; Zhang, Y.; Jiang, B. Searching Configurations in Uncertainty Space: Active Learning of High-Dimensional Neural Network Reactive Potentials. J. Chem. Theory Comput. 2021, 17, 2691–2701.
- Schran, C.; Behler, J.; Marx, D. Automated Fitting of Neural Network Potentials at Coupled Cluster Accuracy: Protonated Water Clusters as Testing Ground. *J. Chem. Theory Comput.* **2020**, *16*, 88–99.

- Berweger, C. D.; van Gunsteren, W. F.; Müller-Plathe, F. Finite Element Interpolation for Combined Classical/Quantum Mechanical Molecular Dynamics Simulations. *J. Comput. Chem.* **1998**, *18*, 1484–1495.
- Nance, J.; Kelley, C. T. A Sparse Interpolation Algorithm for Dynamical Simulations in Computational Chemistry. SIAM J. Sci. Comput. 2015, 37, S137–S156.
- Judd, K. L.; Maliar, L.; Maliar, S.; Valero, R. Smolyak Method for Solving Dynamic Economic Models: Lagrange Interpolation, Anisotropic Grid and Adaptive Domain. J. Econ. Dyn. Control 2014, 44, 92–123.
- Clenshaw, C. W.; Curtis, A. R. A Method for Numerical Integration on an Automatic Computer. *Numer. Math.* **1960**, *2*, 197–205.
- Smolyak, S. A. Quadrature and Interpolation Formulas for Tensor Products of Certain Classes of Functions. *Dokl. Akad. Nauk.* **1963**, *148*, 1042–1045.
- Novak, E.; Ritter, K. Simple Cubature Formulas with High Polynomial Exactness. *Constr.* Approx. **1999**, 15, 499–522.
- Hallatschek, K. Fouriertransformation auf Dünnen Gittern mit Hierarchischen Basen. Numer. Math. 1992, 63, 83–97.
- Nance, J.; Bowman, D. N.; Mukherjee, S.; Kelley, C. T.; Jakubikova, E. Insights into the Spin-State Transitions in  $[Fe(tpy)_2]_2^+$ : Importance of the Terpyridine Rocking Motion. Inorg. Chem. 2015, 54, 11259–11268.
- Morrow, Z.; Stoyanov, M. A Method for Dimensionally Adaptive Sparse Trigonometric Interpolation of Periodic Functions. SIAM J. Sci. Comput. 2020, 42, A2436–A2460.
- Griebel, M.; Hamaekers, J. In *Sparse Grids and Applications Munich 2012*; Garcke, J., Pflüger, D., Eds.; Lect. Notes Comp. Sci.; Springer International Publishing Switzerland, 2014; Chapter 4, pp 75–107.

- Morrow, Z.; Liu, C.; Kelley, C. T.; Jakubikova, E. Approximating Periodic Potential Energy Surfaces with Sparse Trigonometric Interpolation. *J. Phys. Chem. B* **2019**, *123*, 9677–9684.
- Helmberg, G. The Gibbs Phenomenon for Fourier Interpolation. *J. Approx. Theory* **1994**, 78, 41–63.
- Burton, K. A.; Weisman, R. B. Stepwise Photodissociation of Vapor-Phase Azomethane. *J. Am. Chem. Soc.* **1990**, *112*, 1804–1807.
- Andrews, B. K.; Burton, K. A.; Weisman, R. B. Dynamics of the Two-Step Photodissociation of Azomethane. *J. Chem. Phys.* **1992**, *96*, 1111–1120.
- Diau, E. W.-G.; Zewail, A. H. Femtochemistry of trans-Azomethane: A Combined Experimental and Theoretical Study. *ChemPhysChem* **2003**, *4*, 445–456.
- Sellner, B.; Ruckenbauer, M.; Stambolić, I.; Barbatti, M.; Aquino, A. J. A.; Lischka, H. Photodynamics of Azomethane: A Nonadiabatic Surface-Hopping Study. J. Phys. Chem. A 2010, 114, 8778–8785.
- Cattaneo, P.; Persico, M. Semiclassical Simulations of Azomethane Photochemistry in the Gas Phase and in Solution. *J. Am. Chem. Soc.* **2001**, *123*, 7638–7645.
- Gaenko, A.; DeFusco, A.; Varganov, S. A.; Martínez, T. J.; Gordon, M. S. Interfacing the Ab Initio Multiple Spawning Method with Electronic Structure Methods in GAMESS: Photodecay of trans-Azomethane. J. Phys. Chem. A 2014, 118, 10902–10908.
- Liu, R.; Cui, Q.; Dunn, K. M.; Morokuma, K. Ab Initio Molecular Orbital Study of the Mechanism of Photodissociation of Trans-Azomethane. J. Chem. Phys. 1996, 105, 2333— 2345.
- Ruckenbauer, M.; Barbatti, M.; Sellner, B.; Muller, T.; Lischka, H. Azomethane: Nonadia-batic Photodynamical Simulations in Solution. *J. Phys. Chem. A* **2010**, *114*, 12585–12590.

- Cattaneo, P.; Persico, M. Diabatic and Adiabatic Potential-Energy Surfaces for Azomethane Photochemistry. *Theor. Chem. Acc.* **2000**, *103*, 390–398.
- Hare, S. R.; Bratholm, L. A.; Glowacki, D. R.; Carpenter, B. K. Low Dimensional Representations along Intrinsic Reaction Coordinates and Molecular Dynamics Trajectories Using Interatomic Distance Matrices. *Chem. Sci.* 2019, 10, 9954–9968.
- Schmitz, G.; Klinting, E. L.; Christiansen, O. A Gaussian Process Regression Adaptive Density Guided Approach for Potential Energy Surface Construction. *J. Chem. Phys.* **2020**, *153*, 064105.
- Cattaneo, P.; Persico, M. Semiclassical Treatment of the Photofragmentation of Azomethane. Chem. Phys. Lett. 1998, 289, 160–166.
- Stoyanov, M. User Manual: TASMANIAN Sparse Grids; 2015.
- Stoyanov, M. K.; Webster, C. G. A Dynamically Adaptive Sparse Grids Method for Quasi-Optimal Interpolation of Multidimensional Functions. *Comput. Math. Appl.* **2016**, *71*, 2449–2465.
- Stoyanov, M.; Lebrun-Grandie, D.; Burkardt, J.; Munster, D. Tasmanian. 2013; https://github.com/ORNL/Tasmanian.
- Deriglazov, A. Classical Mechanics; Springer-Verlag, Berlin, 2016.
- Lanczos, C. The Variational Principles of Mechanics; Courier Corporation, 2012.
- Wilson, E. B.; Decius, J. C.; Cross, P. C. Molecular Vibrations: The Theory of Infrared and Raman Vibrational Spectra; McGraw-Hill, 1955.
- Verlet, L. Computer "Experiments" on Classical Fluids. I. Thermodynamical Properties of Lennard–Jones Molecules. *Phys. Rev.* **1967**, *159*, 98–103.

- Störmer, C. Sur les trajectoires des corpuscules électrisés dans l'espace sous l'action du magnétisme terrestre, avec application aux aurores boréales. Arch. Sci. Phys. Nat. 1912, 33, 51–69.
- Gautschi, W. Numerical Analysis, 2nd ed.; Birkhäuser Basel, 2012.
- Virtanen, P.; Gommers, R.; Oliphant, T. E.; Haberland, M.; Reddy, T.; Cournapeau, D.; Burovski, E.; Peterson, P.; Weckesser, W.; Bright, J.; van der Walt, S. J.; Brett, M.; Wilson, J.; Millman, K. J.; Mayorov, N.; Nelson, A. R. J.; Jones, E.; Kern, R.; Larson, E.; Carey, C. J.; Polat, İ.; Feng, Y.; Moore, E. W.; VanderPlas, J.; Laxalde, D.; Perktold, J.; Cimrman, R.; Henriksen, I.; Quintero, E. A.; Harris, C. R.; Archibald, A. M.; Ribeiro, A. H.; Pedregosa, F.; van Mulbregt, P.; SciPy 1.0 Contributors, SciPy 1.0: Fundamental Algorithms for Scientific Computing in Python. Nat. Methods 2020, 17, 261–272.
- Powell, M. J. D. An Efficient Method for Finding the Minimum of a Function of Several Variables without Calculating Derivatives. *Comput. J.* **1964**, *7*, 155–162.
- Kelley, C. T. Iterative Methods for Linear and Nonlinear Equations; SIAM, 1995.
- Kelley, C. T. Numerical Methods for Nonlinear Equations. Acta Numer. 2018, 27, 207–287.
- Allen, M. P.; Tildesley, D. J. Computer Simulations of Liquids, 2nd ed.; Oxford University Press, 2017.
- Leimkuhler, B.; Matthews, C. Robust and Efficient Configurational Molecular Sampling via Langevin Dynamics. J. Chem. Phys. 2013, 138, 174102.
- Leimkuhler, B.; Matthews, C. Rational Construction of Stochastic Numerical Methods for Molecular Sampling. *Appl. Math. Res. Express* **2013**, *2013*, 34–56.
- Helgaker, T.; Uggerud, E.; Jensen, H. J. A. Integration of the Classical Equations of Motion on Ab Initio Molecular Potential Energy Surfaces Using Gradients and Hessians: Applica-

- tion to Translational Energy Release upon Fragmentation. *Chem. Phys. Lett.* **1990**, *173*, 145–150.
- Uggerud, E.; Helgaker, T. Dynamics of the Reaction  $CH_2OH^+ \rightarrow CHO^+ + H_2$ . Translational Energy Release from Ab Initio Trajectory Calculations. *J. Am. Chem. Soc.* **1992**, *114*, 4265–4268.
- Frisch, M. J.; Trucks, G. W.; Schlegel, H. B.; Scuseria, G. E.; Robb, M. A.; Cheeseman, J. R.; Scalmani, G.; Barone, V.; Petersson, G. A.; Nakatsuji, H.; Li, X.; Caricato, M.; Marenich, A. V.; Bloino, J.; Janesko, B. G.; Gomperts, R.; Mennucci, B.; Hratchian, H. P.; Ortiz, J. V.; Izmaylov, A. F.; Sonnenberg, J. L.; Williams-Young, D.; Ding, F.; Lipparini, F.; Egidi, F.; Goings, J.; Peng, B.; Petrone, A.; Henderson, T.; Ranasinghe, D.; Zakrzewski, V. G.; Gao, J.; Rega, N.; Zheng, G.; Liang, W.; Hada, M.; Ehara, M.; Toyota, K.; Fukuda, R.; Hasegawa, J.; Ishida, M.; Nakajima, T.; Honda, Y.; Kitao, O.; Nakai, H.; Vreven, T.; Throssell, K.; Montgomery, J. A., Jr.; Peralta, J. E.; Ogliaro, F.; Bearpark, M. J.; Heyd, J. J.; Brothers, E. N.; Kudin, K. N.; Staroverov, V. N.; Keith, T. A.; Kobayashi, R.; Normand, J.; Raghavachari, K.; Rendell, A. P.; Burant, J. C.; Iyengar, S. S.; Tomasi, J.; Cossi, M.; Millam, J. M.; Klene, M.; Adamo, C.; Cammi, R.; Ochterski, J. W.; Martin, R. L.; Morokuma, K.; Farkas, O.; Foresman, J. B.; Fox, D. J. Gaussian 16 Revision A.03. 2016; Gaussian Inc., Wallingford, CT.
- Becke, A. D. Density-Functional Thermochemistry. III. The Role of Exact Exchange. *J. Chem. Phys.* **1993**, *98*, 5648–5652.
- Becke, A. D. A New Mixing of Hartree-Fock and Local Density-Functional Theories. *J. Chem. Phys.* **1993**, *98*, 1372–1377.
- Lee, C.; Yang, W.; Parr, R. G. Development of the Colle-Salvetti Correlation-Energy Formula into a Functional of the Electron Density. *Phys. Rev. B* **1988**, *37*, 785–789.
- Stephens, P. J.; Devlin, F. J.; Chabalowski, C. F.; Frisch, M. J. Ab Initio Calculation of

- Vibrational Absorption and Circular Dichroism Spectra Using Density Functional Force Fields. J. Phys. Chem. 1994, 98, 11623–11627.
- Krishnan, R.; Binkley, J. S.; Seeger, R.; Pople, J. A. Self-Consistent Molecular Orbital Methods. XX. A Basis Set for Correlated Wave Functions. J. Chem. Phys. 1980, 72, 650–654.
- Bauernschmitt, R.; Ahlrichs, R. Stability Analysis for Solutions of the Closed Shell Kohn–Sham Equation. J. Chem. Phys. 1996, 104, 9047–9052.
- Li, X.; Frisch, M. J. Energy-Represented Direct Inversion in the Iterative Subspace within a Hybrid Geometry Optimization Method. *J. Chem. Theory Comput.* **2006**, *2*, 835–839.
- Towns, J.; Cockerill, T.; Dahan, M.; Foster, I.; Gaither, K.; Grimshaw, A.; Hazlewood, V.; Lathrop, S.; Lifka, D.; Peterson, G. D.; Roskies, R.; Scott, J.; Wilkins-Diehr, N. XSEDE: Accelerating Scientific Discovery. Comput. Sci. Eng. 2014, 16, 62–74.
- Nystrom, N. A.; Levine, M. J.; Roskies, R. Z.; Scott, J. R. *Proc. XSEDE Conf.*; Association for Computing Machinery: New York, 2015.
- Münster, A. Statistical Thermodynamics; Springer-Verlag, Berlin, 1969.
- Tully, J. C. Molecular Dynamics with Electronic Transitions. J. Chem. Phys. 1990, 93, 1061–1071.
- Nance, J. D. Investigating Molecular Dynamics with Sparse Grid Surrogate Models. Ph.D. thesis, North Carolina State University, 2015.

## Graphical TOC Entry

